VOL. 16, NO. 6, MARCH 2021 ISSN 1819-6608
ARPN Journal of Engineering and Applied Sciences

www.arpnjournals.com

THE INFLUENCE OF METACHRONAL BEATING OF CILIA ON THE BEHAVIOR OF BLOOD FLOWING THROUGH ELASTIC STENOSED ARTERIES

M. A. El Kot[1,2]
[1]Department of Mathematics, College of Sciences and Arts, Dhahran Aljanoub, King Khalid University, Saudi Arabia
[2]Department of Mathematics and Computer Science, Faculty of Science, Suez University, Suez, Egypt
E-Mail: melkot@kku.edu.sa

ABSTRACT

The influence of the metachronal beating of cilia, heat transfer phenomenon, oblique magnetic field, and Hall currents on blood flowing inside an isotropically stenosed elastic artery were investigated analytically. All physical parameters associated with blood flow properties were studied and discussed graphically for both ciliated-free isotropic artery and ciliated-tethered artery. The results obtained in this study showed that the velocity, the distribution of wall shear stress, and the resistance are higher for free isotropic artery model than that for tethered artery model. The distribution of wall shear stress increases with the cilia position increasing and it decreases by increasing the eccentricity of the elliptic path whereas the resistance impedance has inverse trend. Furthermore, the streamlines patterns illustrating the features of the ciliary motion have been plotted for various imbedded flow parameters.

Keywords: metachronal beating of cilia, oblique magnetic field, isotropic elastic arteries, vertical annulus.

1. INTRODUCTION

Atherosclerosis occurs when the normal state of blood flow changes to a disordered state due to a narrowing of the arteries. Cholesterol is one of the most important causes of narrowing of the arteries, as it increases the accumulation of plaque layers along the inner lining of the arteries that grow inside and restrict the flow of blood. The careful study of blood flow properties with full awareness of the dynamic features of vascular walls helps in the description and treatment of vascular diseases and helps medical engineers in the design and improvement of artificial limbs [1].

Flagella and cilia are filamentous extensions of the cell surface surrounded by a membrane that is an extension of the cell membrane. The flagella and cilia are similar in their general structure, but the flagella are longer and less numerous than the cilia. The flagella and cilia are composed of two main molecules, the basal body, and the central axial thread. Flagella and cilia are found in animals and unicellular and multicellular plants such as epithelium cells lining the trachea or ovarian canal and there are flagella that carry tails like sperm. Some people may think that cilia have no value, but their absence leads to many diseases, so what are their benefits. In biology, the movement of dynamic cilia helps in transporting biological fluids. The movement of biological fluids resulting from the mass shaking of a group of cilia represent the main manifestation of blood pumping and peristalsis. Cilia play an active role in the cell's life cycle and organism's growth, as in the heart. Cilia have the property of selectively allowing some proteins and play an important role in cellular communication. Cilia can remove the trachea mucus in the respiratory tract as well as Transfer of ovulatory mucus and the ovum into the oviduct of the female reproductive pathway. Furthermore, cilia located in brain cells are believed to be contribute to the transmission of cerebrospinal liquid [2, 3, 4]. Cilia, hair like moving appendages, appear in the respiratory and digestive systems of humans and in the nervous system of all animals. Cilia mobility plays a vital role in all physiological processes such as movement, nutrition, circulation, respiration, and reproduction [5]. Flagella or cilia move quickly forward and backward to create a fast movement that pushes the cell forward. The flagella move in a wavy movement, while the cilia move in a gradual harmonic movement, where some cilia fold in this direction, then return to their initial position to fold again gradually. The cilia move within the axial circumference in one direction by a sliding way on the outer surface of the microbial tubes by adenosine triphosphate (ATP) to activate dynein protein [6]. An approximate size, structure, and the patterns of motion of cilium are shown in Figure-1.

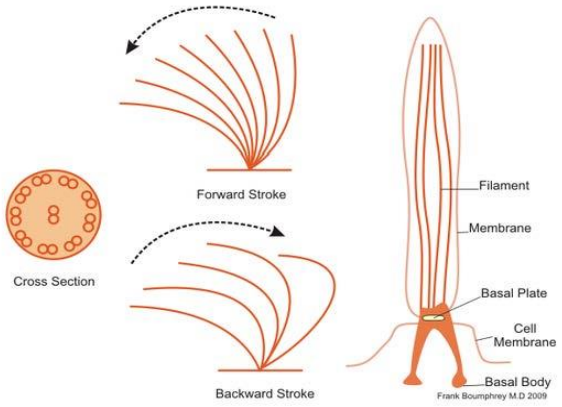

Figure-1. The structural shape of the cilia.

The examination of heat transfer effectiveness on bio-fluids theoretically or experimentally attracted the attention of many investigators. The property of thermal transfer of blood has an essential role in the assimilation

and prosperity of arterial diseases. The important contributions of recent years to the characteristic of heat transfer related to biological fluids were referenced in the literature [7-15].

The objective of this paper is to study the behavior of blood transport inside an artery with time-variant overlapping Stricture in a vertical annulus, with the consideration of metachronal wave motion due to cilia and the effect of elastic wall properties.

2. PROBLEM FORMULATION

Assuming an incompressible viscous Newtonian fluid fills a closed cylindrical viscoelastic narrowed tube represent artery of length L, radius R_o, and its inner surface contains cilia. Another solid circular cylinder catheter with radius $(a<<1)$ is inserted into the tube moving with constant velocity V_o. Using the cylindrical polar coordinates system (r,θ,z), consider the system is influenced by the gravitational force in the negative z-direction, and the fluid is subjected to an oblique magnetic field $\left(\vec{B}=B_o\cos\alpha\,\hat{e}_z+B_o\sin\alpha\,\hat{e}_r\right)$ where B_o refers to the constant part of the field, α is the inclination angle of magnetic field. Applying, the thermal transfer feature by donating a temperature T_o to the arterial wall while catheter wall maintains the temperature of T_1.

The geometrical shape of the constricted region is taken as (see Figure-2) [16].

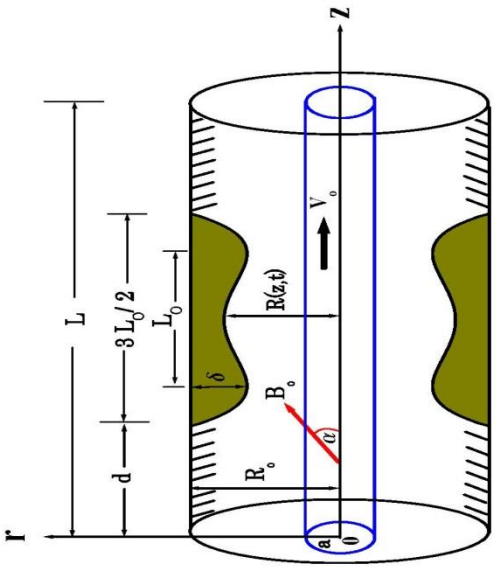

Figure-2. Graphical scheme of ciliated narrowed artery.

$$\frac{R(z,t)}{R_o}=\left[1-\frac{\delta(z-d)}{R_o\,L_o}\left\{11-\frac{94(z-d)}{3L_o}+\frac{32(z-d)^2}{L_o^2}-\frac{32(z-d)^3}{3L_o^3}\right\}\right]\Omega(t) \qquad d\le z\le d+\frac{3L_o}{2} \tag{2.1}$$

$$=\Omega(t) \qquad \text{otherwise,}$$

and the function $\Omega(t)$ can be written as

$$\Omega(t)=1-b(\cos\omega t-1)\exp[-b\omega t], \tag{2.2}$$

where $\frac{3L_o}{2}$ is the length of overlapping stenosis, d is the site of the stenosis, b is the amplitude of artery radius, ω is the angular frequency of forced oscillation, and t represent the time.

The mathematical description of the problem may be listed by the following governing equations:

$$\vec{\nabla}\cdot\vec{V}=0, \tag{2.3}$$

$$\rho\left(\frac{\partial\vec{V}}{\partial t}+\vec{V}\cdot\nabla\vec{V}\right)=-\vec{\nabla}p+\mu\nabla^2\vec{V}+\vec{J}\times\vec{B}-\rho g\gamma\left(\vec{T}-\vec{T}_o\right), \tag{2.4}$$

$$\rho c_p\left(\frac{\partial\vec{T}}{\partial t}+\vec{V}\cdot\nabla\vec{T}\right)=K\nabla^2\vec{T}+\Phi, \tag{2.5}$$

$$\vec{\nabla}\times\vec{B}=\mu_e\vec{J},\ \vec{\nabla}\cdot\vec{B}=0,\ \vec{\nabla}\times\vec{E}=0,\ \vec{\nabla}\cdot\vec{J}=0, \tag{2.6}$$

$$\vec{J}=\sigma\left[\vec{E}+\vec{V}\times\vec{B}\right]-\frac{\sigma}{\nu n_e}\vec{J}\times\vec{B}. \tag{2.7}$$

Where μ is fluid viscosity, ρ is fluid density, $\vec{V}$ is the velocity vector, $\vec{B}$ is the magnetic field vector, $\vec{E}$ is electric field vector, $\vec{J}$ is current density vector, $\vec{T}$ is the temperature vector, g represent the acceleration of gravity, γ is the thermal expansion coefficient, K is the thermal conductivity, c_p is the specific heat at fixed pressure, Φ symbolize to the frictional heating, σ is electrical conductivity of the fluid, ν is electric charge, n_e is number density of electrons, and μ_e is magnetic permeability.

The equations describing the arterial wall movement [1], [17], [18], [19]]:

$$M_o\frac{\partial^2\zeta}{\partial t^2}+C_l\frac{\partial\zeta}{\partial t}+K_l\zeta=-\mu\left(\frac{\partial V_z}{\partial r}+\frac{\partial V_r}{\partial z}\right)\Big|_{r=R_o}+\frac{\partial\eta}{\partial z}\left(\frac{T_{to}-T_{\theta o}}{R_o}\right)+\frac{E_t h}{1-\sigma_\theta\sigma_t}\left(\frac{\sigma_\theta}{R_o}\frac{\partial\eta}{\partial z}+\frac{\partial^2\zeta}{\partial z^2}\right), \tag{2.8}$$

$$M_o\frac{\partial^2\eta}{\partial t^2}+C_r\frac{\partial\eta}{\partial t}+K_r\eta=\left(p-2\mu\frac{\partial V_r}{\partial r}\right)\Bigg|_{r=R_o}+\frac{\eta}{R_o^2}T_{\theta o}+T_{to}\frac{\partial^2\eta}{\partial z^2}-\frac{E_\theta h}{R_o\left(1-\sigma_\theta\sigma_t\right)}\left(\frac{\eta}{R_o}+\sigma_t\frac{\partial\zeta}{\partial z}\right),\tag{2.9}$$

where V_r and V_z are radial and axial velocities consecutively, In writing equations (2.8) and (2.9), $M_o=\rho_o h+M_a$ where ρ_o is mass density, h is artery wall thickness, and M_a is the extra mass of the mechanical form. $\left(T_{to},T_{\theta o}\right)$ are initial viscoelastic stress components acting along longitudinal and circumferential directions consecutively. K_l,C_l are spring and friction coefficients in longitudinal direction consecutively also K_r,C_r are the same in radial direction. E_θ and E_t are Young's moduli also σ_θ and σ_t are Poisson's ratios in circumferential and longitudinal directions consecutively.

Following Sleigh (1968) [20], the cilia move in elliptical paths and the radial position of a cilia tip $\eta\left(z,t\right)$ is assumed to be written as

$$\eta\left(z,t\right)=R_o+\varphi R_o\cos\left(\frac{2\pi\left(z-u_o t\right)}{\chi}\right),\tag{2.10}$$

and the horizontal position of a cilia tip $\zeta\left(z,t\right)$ is given as

$$\zeta\left(z,t\right)=Z_o+e\varphi R_o\sin\left(\frac{2\pi\left(z-u_o t\right)}{\chi}\right),\tag{2.11}$$

where φ is the length of cilia, e measure the eccentricity of elliptical path, Z_o is the position of cilia, u_o is the fluid mean velocity, and χ is the length of the metachronal wave.

The boundary conditions are:

$$V_r=0,\ V_z=V_o,\ T=T_o\quad\text{on } r=a,\tag{2.12}$$

$$V_r=\frac{\partial\eta}{\partial t},\ V_z=\frac{\partial\zeta}{\partial t},\ T=T_1\ \text{on } r=R\left(z,t\right).\tag{2.13}$$

Assume that $V=\left(V_r,0,V_z\right)$ and using the following non-dimensional variables:

$$\begin{aligned}
&r=R_o r',\ z=L_o z',\ \omega=\frac{u_o}{L_o}\omega',\ \zeta=L_o\zeta',\ \eta=L_o\eta',V_r=\frac{\delta u_o}{L_o}V_r',V_z=u_oV_z',R=R_oR',\\
&t=\frac{L_o}{u_o}t',\ p=\frac{u_oL_o\mu}{R_o^2}p',\ V_o=u_oV_o',\ M_o=\rho R_oM_o',\ C_l=\rho u_oC_l',\ C_r=\rho u_oC_r',\\
&K_l=\frac{\rho u_o^2}{R_o}K_l',\ K_r=\frac{\rho u_o^2}{R_o}K_r',T_{to}=\rho u_o^2R_oT_{to}',\ T_{\theta o}=\rho u_o^2R_oT_{\theta o}',\ h=R_oh',\ E_t=\rho u_o^2E_t',\\
&E_\theta=\rho u_o^2E_\theta',\ T=T_o+\left(T_1-T_o\right)\Theta,Z_o=L_oZ_o',\ \chi=L_o\chi',\ d^*=\frac{d}{L_o},\varepsilon=\frac{a}{R_o},\ L^*=\frac{L}{L_o}.
\end{aligned}\tag{2.14}$$

Using equation (2.14), the equations (2.3-2.5) and (2.8-2.11) after dropping the dashes become:

$$\delta^*\left(\frac{\partial V_r}{\partial r}+\frac{V_r}{r}\right)+\frac{\partial V_z}{\partial z}=0,\tag{2.15}$$

$$\begin{aligned}
R_e\delta^*\Sigma^3\left(\frac{\partial V_r}{\partial t}+\delta^*V_r\frac{\partial V_r}{\partial r}+V_z\frac{\partial V_r}{\partial z}\right)=&-\frac{\partial p}{\partial r}+\delta^*\Sigma^2\left(\frac{\partial^2V_r}{\partial r^2}+\frac{1}{r}\frac{\partial V_r}{\partial r}-\frac{V_r}{r^2}+\Sigma^2\frac{\partial^2V_r}{\partial z^2}\right)\\
&+H_a^2\Sigma\,\Phi\cos\alpha\left(V_z\sin\alpha-\delta^*\Sigma V_r\cos\alpha\right)
\end{aligned}\tag{2.16}$$

$$\begin{aligned}
R_e\Sigma\left(\frac{\partial V_z}{\partial t}+\delta^*V_r\frac{\partial V_z}{\partial r}+V_z\frac{\partial V_z}{\partial z}\right)=&-\frac{\partial p}{\partial z}+\frac{\partial^2V_z}{\partial r^2}+\frac{1}{r}\frac{\partial V_z}{\partial r}+\Sigma^2\frac{\partial^2V_z}{\partial z^2}\\
&-H_a^2\Phi\sin\alpha\left(V_z\sin\alpha-\delta^*\Sigma V_r\cos\alpha\right)+G_r\Theta,
\end{aligned}\tag{2.17}$$

$$R_ep_r\Sigma\left(\frac{\partial\Theta}{\partial t}+\delta^*V_r\frac{\partial\Theta}{\partial r}+V_z\frac{\partial\Theta}{\partial z}\right)=\frac{\partial^2\Theta}{\partial r^2}+\frac{1}{r}\frac{\partial\Theta}{\partial r}+\Sigma^2\frac{\partial^2\Theta}{\partial z^2}+\beta,\tag{2.18}$$

$$\Sigma^2M_o\frac{\partial^2\zeta}{\partial t^2}+\Sigma C_l\frac{\partial\zeta}{\partial t}+K_l\zeta=-\frac{\Sigma}{R_e}\left(\frac{\partial V_z}{\partial r}+\delta^*\Sigma^2\frac{\partial V_r}{\partial z}\right)\Bigg|_{r=1}+\Sigma\frac{\partial\eta}{\partial z}\left(T_{to}-T_{\theta o}\right)+\frac{\Sigma E_th}{1-\sigma_\theta\sigma_t}\left(\sigma_\theta\frac{\partial\eta}{\partial z}+\Sigma\frac{\partial^2\zeta}{\partial z^2}\right),\tag{2.19}$$

$$\Sigma^2M_o\frac{\partial^2\eta}{\partial t^2}+\Sigma C_r\frac{\partial\eta}{\partial t}+K_r\eta=\frac{1}{R_e}\left(p-2\delta^*\Sigma^2\frac{\partial V_r}{\partial r}\right)\Bigg|_{r=1}+T_{\theta o}\eta+\Sigma^2T_{to}\frac{\partial^2\eta}{\partial z^2}-\frac{E_\theta h}{1-\sigma_\theta\sigma_t}\left(\eta+\Sigma\sigma_t\frac{\partial\zeta}{\partial z}\right).\tag{2.20}$$

Let us simplify the equations of motion for mild stenosis by adopting the two conditions $\left(\delta^* = \frac{\delta}{R_o} << 1\right)$ and $\left(\Sigma = \frac{R_o}{L_o} \approx o(1)\right)$ [21]. Under these assumptions, the equations (2.15-2.20) are as follows

$$\frac{\partial p}{\partial r} = 0, \tag{2.21}$$

$$\frac{\partial p}{\partial z} = \frac{\partial^2 V_z}{\partial r^2} + \frac{1}{r}\frac{\partial V_z}{\partial r} - \frac{H_a^2 \sin^2 \alpha \; V_z}{1+S^2} + G_r \Theta, \tag{2.22}$$

$$\frac{1}{r}\frac{\partial}{\partial r}\left(r\frac{\partial \Theta}{\partial r}\right) + \beta = 0, \tag{2.23}$$

$$K_l \zeta = 0, \tag{2.24}$$

$$p(z,t) = R_e\left(K_r - T_{\theta o} + \frac{E_\theta h}{1 - n\sigma_\theta^2}\right)\eta(z,t), \tag{2.25}$$

where $R_e = \frac{\rho \, u_o R_o}{\mu}$ is Reynolds number, $H_a = \sqrt{\frac{\sigma}{\mu}}\, B_o R_o$ is the Hartmann number, $S = \frac{\sigma \, B_o}{\nu \, n_e}$ is the Hall parameter, $G_r = \frac{\rho g \gamma R_o^2 (T_1 - T_o)}{u_o \, \mu}$ is the Grashof number, $P_r = \frac{c_p \, \mu}{K}$ is the Prandtl number of the fluid, $\beta = \frac{Q_o \, R_o^2}{(T_1 - T_o)K}$ is the heat source/sink parameter and $n = \frac{\sigma_t}{\sigma_\theta}$ is the degree of anisotropy of the vessel wall.

The radial and horizontal positions of a cilia tip (dropping dashes) become

$$\eta(z,t) = \Sigma + \varphi\Sigma\cos\left(\frac{2\pi(z-t)}{\chi}\right), \tag{2.26}$$

$$\zeta(z,t) = Z_o + e\varphi\Sigma\sin\left(\frac{2\pi(z-t)}{\chi}\right), \tag{2.27}$$

The corresponding boundary conditions (dropping dashes):

$$V_z = V_o, \; \Theta = 1 \quad \text{on} \; r = \varepsilon \tag{2.28}$$

$$V_z = \frac{\partial \zeta}{\partial t}, \; \Theta = 0 \quad \text{on} \; r = R(z,t) \tag{2.29}$$

$$R(z,t) = \begin{cases} \left[1 - \delta^*\left(z - d^*\right)\left\{11 - \frac{94\left(z-d^*\right)}{3} + 32\left(z-d^*\right)^2 - \frac{32\left(z-d^*\right)^3}{3}\right\}\right]\Omega(t) & d^* \le z \le d^* + \frac{3L_o}{2} \\ = \Omega(t) & \text{otherwise} \end{cases} \tag{2.30}$$

2.1 SOLUTION OF THE PROBLEM

Form equation (2.24) we can note that $\zeta = 0$ where $K_l \neq 0$ and by using equations (2.25), (2.26) and (2.27), we can find the gradient of the fluid pressure in the form

$$\frac{dp}{dz} = \frac{2\pi Z_o R_e}{e\chi}\left(K_r - T_{\theta o} + \frac{E_\theta h}{1 - n\sigma_\theta^2}\right). \tag{2.31}$$

Applying the boundary conditions, we can write axial velocity, and temperature as follow

$$\begin{aligned} V_z(r,z,t) = \frac{1}{m^2 a_{11}}\Bigg[& \frac{dp}{dz}\left\{-a_{11} + a_{12} I_o(mr) + a_{13} K_o(mr)\right\} + G_r\left\{a_{11}\beta + a_{14} I_o(mr) + a_{15} K_o(mr)\right. \\ & + a_{15} K_o(mr) + a_{16}\left(a_{17}\ln(r) - \beta\left(r^2 - \varepsilon^2\right)\ln(R) + \left(\beta\left(r^2 - R^2\right) - 4\right)\ln(\varepsilon)\right\} \\ & \left. + m^2 V_o\left\{K_o(mR) I_o(mr) - I_o(mR) K_o(mr)\right\}\right], \end{aligned} \tag{2.32}$$

$$\Theta(r,z,t) = \frac{1}{4\ln\left(\frac{\varepsilon}{R}\right)}\left[-\beta r^2 \ln\left(\frac{\varepsilon}{R}\right) + \left(\beta\left(\varepsilon^2 - R^2\right) - 4\right)\ln(r) + \beta\left(R^2\ln(\varepsilon) - \varepsilon^2\ln(R)\right) + 4\ln(\varepsilon)\right], \tag{2.33}$$

where $m=\sqrt{\frac{H_a^2\sin^2\alpha}{1+S^2}}$, $I_o(mr)$ and $K_o(mr)$ are modified Bessel functions of zeroth – order and the coefficients $a_{1i}\,(i=1,2,3,4,5,6,7)$ are given by

$$a_{11}=K_o(mR)I_o(m\varepsilon)-I_o(mR)K_o(m\varepsilon),\ a_{12}=K_o(mR)-K_o(m\varepsilon),\quad (2.34)$$
$$a_{13}=I_o(m\varepsilon)-I_o(mR),\ a_{14}=(1+\beta)K_o(m\varepsilon)-\beta K_o(mR),$$
$$a_{15}=-(1+\beta)I_o(m\varepsilon)+\beta I_o(mR),\ a_{16}=\frac{a_{11}}{4\ln\left(\frac{R}{\varepsilon}\right)},\ a_{17}=4+\beta\left(R^2-\varepsilon^2\right),$$

Using equation (2.32), the wall shear stress distribution can be written as follow

$$\tau_R=-\left.\frac{\partial V_z}{\partial r}\right|_{r=R(z,t)},\quad (2.35)$$

The corresponding stream function $\left(V_z=\frac{1}{r}\frac{\partial\psi}{\partial r}\ \text{with}\ \psi=0\ \text{at}\ r=\varepsilon\right)$ is

$$\begin{aligned}\psi(r,z,t)=\frac{1}{m^2a_{11}}\Bigg[&\frac{dp}{dz}\left\{-a_{11}\left(\frac{r^2-\varepsilon^2}{2}\right)+a_{12}\left(\frac{rI_o(mr)-\varepsilon I_o(m\varepsilon)}{m}\right)+a_{13}\left(\frac{rK_o(mr)-\varepsilon K_o(m\varepsilon)}{m}\right)\right\}\\&+G_r\left\{a_{11}\beta\left(\frac{r^2-\varepsilon^2}{2}\right)+a_{14}\left(\frac{rI_o(mr)-\varepsilon I_o(m\varepsilon)}{m}\right)+a_{15}\left(\frac{rK_o(mr)-\varepsilon K_o(m\varepsilon)}{m}\right)\right.\\&+a_{16}\left(\frac{a_{17}}{4}\left(r^2\left(\ln\left(r^2\right)-1\right)-\varepsilon^2\left(\ln\left(\varepsilon^2\right)-1\right)\right)-\beta\frac{\left(r^2-\varepsilon^2\right)^2}{4}\ln(R)\right.\\&\left.\left.+\left(\frac{\left(r^2-\varepsilon^2\right)\left(\beta\left(r^2+\varepsilon^2-2R^2\right)-4\right)}{4}\right)\ln(\varepsilon)\right\}\\&+m^2V_o\left\{\frac{K_o(mR)}{m}\left(rI_o(mr)-\varepsilon I_o(m\varepsilon)\right)-\frac{I_o(mR)}{m}\left(rK_o(mr)-\varepsilon K_o(m\varepsilon)\right)\right\}\Bigg],\end{aligned}\quad (2.36)$$

The fluid flow rate Q can be calculated by where

$$Q=2\pi\int_{\varepsilon}^{R}rV_z\,dr=\left(-\frac{dp}{dz}\right)\frac{1}{F(z,t)},\quad (2.37)$$

$$\begin{aligned}F(z,t)=a_{11}\Bigg/\Bigg[&-a_{11}\left(\frac{R^2-\varepsilon^2}{2}\right)+a_{12}\left(\frac{RI_o(mR)-\varepsilon I_o(m\varepsilon)}{m}\right)+a_{13}\left(\frac{RK_o(mR)-\varepsilon K_o(m\varepsilon)}{m}\right)\Bigg\}\\&+\frac{G_r}{\left(\frac{dp}{dz}\right)}\left\{a_{11}\beta\left(\frac{R^2-\varepsilon^2}{2}\right)+a_{14}\left(\frac{RI_o(mR)-\varepsilon I_o(m\varepsilon)}{m}\right)+a_{15}\left(\frac{RK_o(mR)-\varepsilon K_o(m\varepsilon)}{m}\right)\right.\\&+a_{16}\left(\frac{a_{17}}{4}\left(R^2\left(\ln\left(R^2\right)-1\right)-\varepsilon^2\left(\ln\left(\varepsilon^2\right)-1\right)\right)-\beta\frac{\left(R^2-\varepsilon^2\right)^2}{4}\ln(R)+\left(\frac{\left(R^2-\varepsilon^2\right)\left(\beta\left(\varepsilon^2-R^2\right)-4\right)}{4}\right)\ln(\varepsilon)\right\}\\&\left.+\frac{m^2V_o}{\left(\frac{dp}{dz}\right)}\left\{\frac{K_o(mR)}{m}\left(RI_o(mR)-\varepsilon I_o(m\varepsilon)\right)\right)-\frac{I_o(mR)}{m}\left(RK_o(mR)-\varepsilon K_o(m\varepsilon)\right)\right\}\Bigg].\end{aligned}\quad (2.38)$$

The pressure drop across the arterial length is obtain in the from The expression for resistance impedance is

$$\Delta p=\int_0^{L^*}\left(-\frac{dp}{dz}\right)dz=Q\int_0^{L^*}F(z,t)\,dz.\quad (2.39)$$

$$\lambda = \frac{\Delta p}{Q} = \frac{m^2}{2\pi}\left[\int_0^{d^*} F(z,t)\Big|_{R=\Omega(t)}\, dz + \int_0^{d^*+\frac{3}{2}} F(z,t)\, dz + \int_{d^*+\frac{3}{2}}^{L^*} F(z,t)\Big|_{R=\Omega(t)}\, dz\right] \quad (2.40)$$

$$= \frac{m^2}{2\pi}\left[F(z,t)\Big|_{R=\Omega(t)}\left(L^* - \frac{3}{2}\right) + \int_0^{d^*+\frac{3}{2}} F(z,t)\, dz\right],$$

3. DISCUSSION OF NUMERICAL RESULTS

Axial velocity V_z, temperature distribution θ, resistance impedance λ, and the wall shear stress τ_w were calculated analytically. To discuss the implications of Hartmann number H_a, the angle of inclination of the magnetic field α, Grashof number G_r, heat source parameter β, the maximum height of constriction δ^*, artery amplitude parameter b, catheter velocity V_o, the non-dimensional radius of catheter ε, the anisotropy of the arterial wall n, initial circumferential viscoelastic stress $T_{\theta o}$, circumferential Poisson's ratio σ_θ, the elastic constraints of total tethering K_r, cilia position Z_o, and the eccentricity of the elliptical path e, We will exploit the following experimental information [[1],[17],[19], [22]]:

$R_e = 1,\ L_o = 1,\ d^* = 0.75,\ \chi = 0.0006,\ \omega = 7.854,\ E_\theta = 40,\ h = 0.001,\ H_a > \sqrt{2},$
$\varepsilon = 0.23$ upto $0.44,\ G_r = 0$ upto $9,\ \beta < 0$ (heat sink) or $\beta \geq 0$ (absence or presence of heat source)

The initial circumferential viscoelastic stress $T_{\theta o}$ was calculated by Atabek and Lew [19]. The effectiveness of circumferential Poisson's ratio σ_θ, and the elastic constraints of total tethering K_r were analyzed by Womersley [23]. The experimental data of the position of cilia Z_o, and the eccentricity of the elliptical path e were investigated by Agrawal and Anawaruddin [5]. Data representing the free isotropic artery is $(T_{\theta o} = 0,\ \sigma_\theta = 0.5,\ n = 1,\ K_r = 0)$ where the artery is initially unstressed [23]. Data representing the tethered artery is $(T_{\theta o} = 0.1,\ \sigma_\theta = 0.51,\ n = 0.63,\ K_r = 1.6)$ [[1], [17], [22], [23]].

Figures (3-5) indicate the influence of the axial velocity V_z by heat source parameter β, Grashof number G_r (free convection parameter), the position of cilia Z_o, the eccentricity of elliptical path e, catheter velocity V_o, the radius of catheter ε, the elastic constraints of total tethering K_r, initial circumferential viscoelastic stress $T_{\theta o}$, the anisotropy of the arterial wall n, and Poisson's ratio σ_θ. Figures (3-5) show that V_z increase by increasing β, G_r, e, and ε whilst it decreases by increasing Z_o, and V_o. Also, Figures (3-5) illustrate that the axial velocity curves inside free artery are always higher than these in tethered artery. The influence of elastic parameters $(T_{\theta o},\ \sigma_\theta,\ n,\ K_r)$ on the axial velocity V_z has been presented graphically in Figures (6-7). It is noticed that the velocity varies directly with the initial circumferential viscoelastic stress $T_{\theta o}$ and increase significantly as the initial circumferential viscoelastic stress increase while it decreases as the anisotropy of the arterial wall n, Poisson's ratio σ_θ and the elastic constraints of total tethering K_r increases.

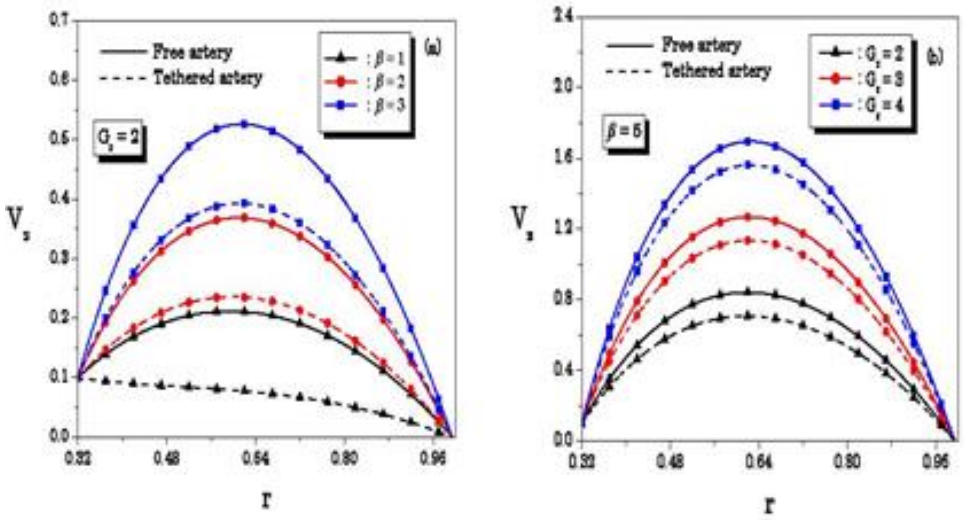

Figure-3. Variation of velocity profiles V_z for β and G_r at $t = 0.5,\ z = 1.2,\ \delta^* = 0.1,\ H_a = 2,\ \alpha = 45^o,\ S = 0.5,\ \varepsilon = 0.32,$ $V_o = 0.1,\ e = 0.3,\ Z_o = 0.0001$ (panels (a) and (b) respectively).

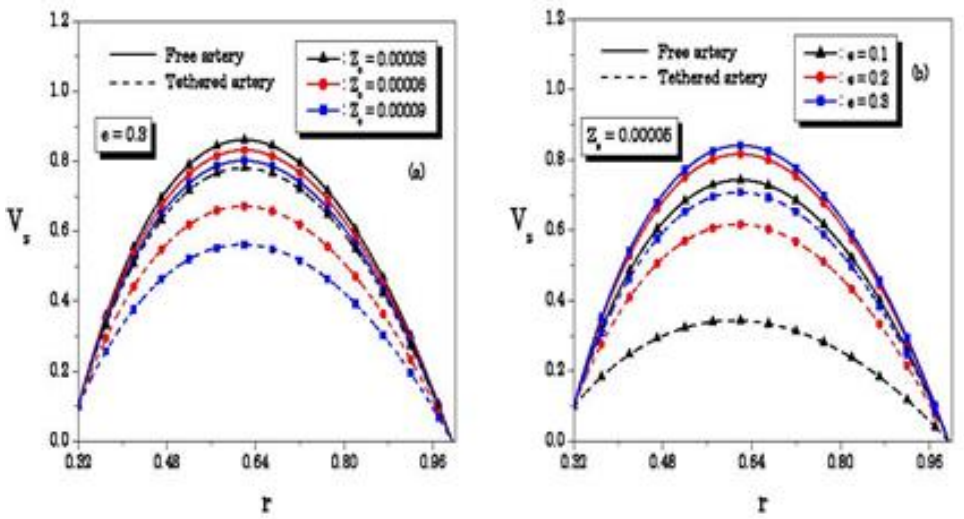

Figure-4. Variation of velocity profiles V_z for Z_o and e at $t = 0.5,\ z = 1.2,\ \delta^* = 0.1,\ H_a = 2, \alpha = 45^o,\ S = 0.5,\ \varepsilon = 0.32,$ $V_o = 0.1,\ \beta = 5,\ G_r = 2$ (panels (a) and (b) respectively).

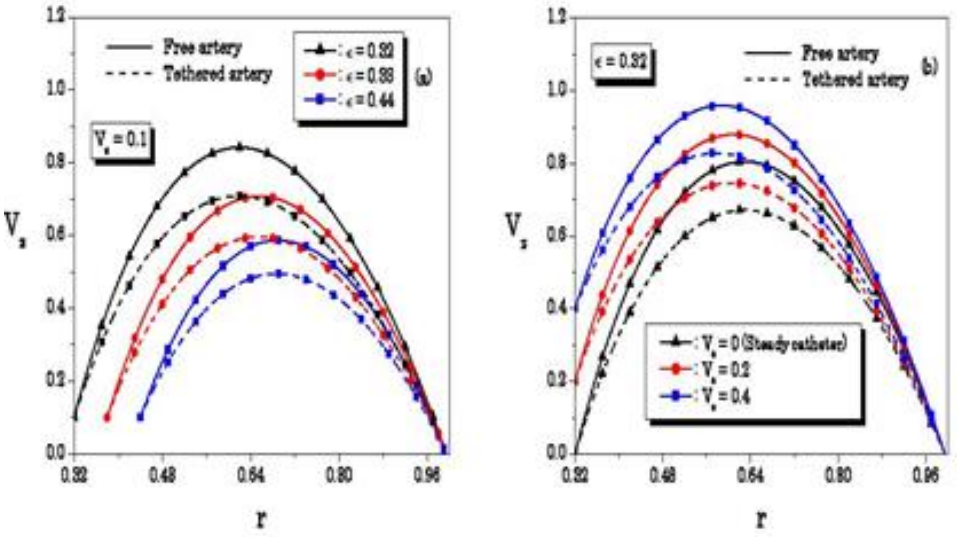

Figure-5. Variation of velocity profiles V_z for ε and V_o at $t = 0.5,\ z = 1.2,\ \delta^* = 0.1,\ H_a = 2, \alpha = 45^o,\ S = 0.5,\ \beta = 5,$ $G_r = 2,\ e = 0.3,\ Z_o = 0.0001$ (panels (a) and (b) respectively).

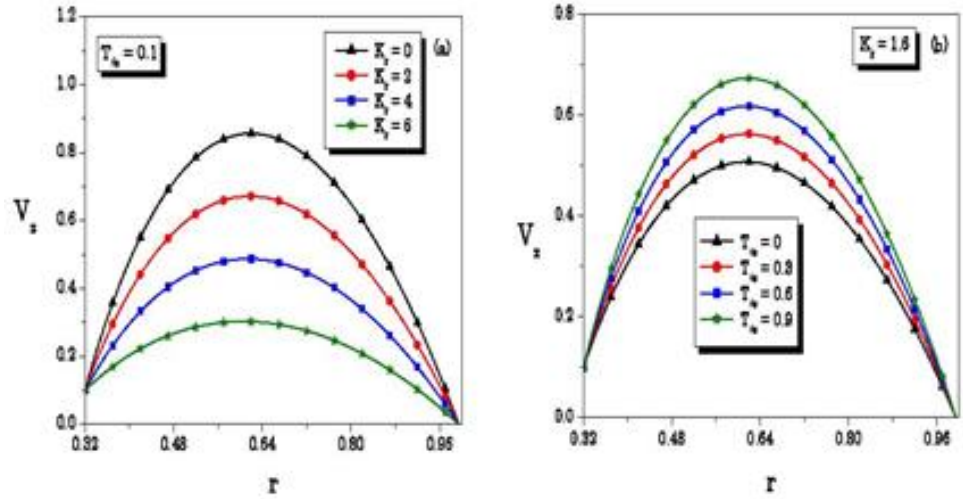

Figure-6. Variation of velocity profiles V_z for K_r and T_θ at $t = 0.5,\ z = 1.2,\ \delta^* = 0.1,\ H_a = 2, \alpha = 45^o,\ S = 0.5,\ \varepsilon = 0.32,\ V_o = 0.1,$ $e = 0.3,\ Z_o = 0.0001,\ \beta = 5,\ G_r = 2,\ \ n = 0.63,\ \ \sigma_\theta = 0.51$ (panels (a) and (b) respectively).

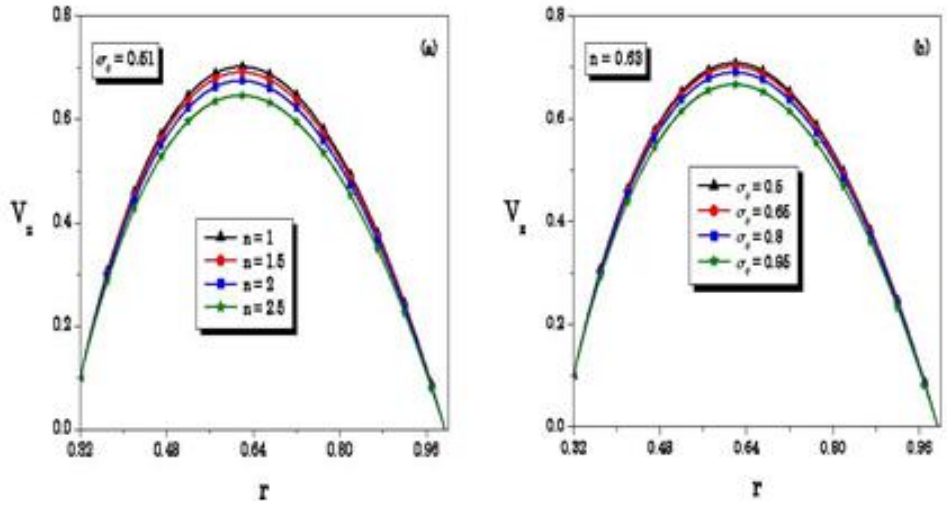

Figure-7. Variation of velocity profiles V_z for n and at $t = 0.5,\ z = 1.2,\ \delta^* = 0.1,\ H_a = 2,\ \alpha = 45^o,\ S = 0.5,$ $\varepsilon = 0.32,\ V_o = 0.1,\ e = 0.3,\ Z_o = 0.0001,\ \beta = 5,\ G_r = 2,\ K_r = 1.6,\ T_\theta = 0.1$ (panels (a) and (b) respectively).

In Figures (8-9), it is noticed that the distribution of wall shear stress τ_w increases as Grashof number G_r, heat source parameter β, and the position of cilia Z_o increases while it decreases by increasing the eccentricity of elliptical path e. Also, the dimensionless wall shear stress results of the free artery model are higher in comparison to the results in case of the tethered artery model.

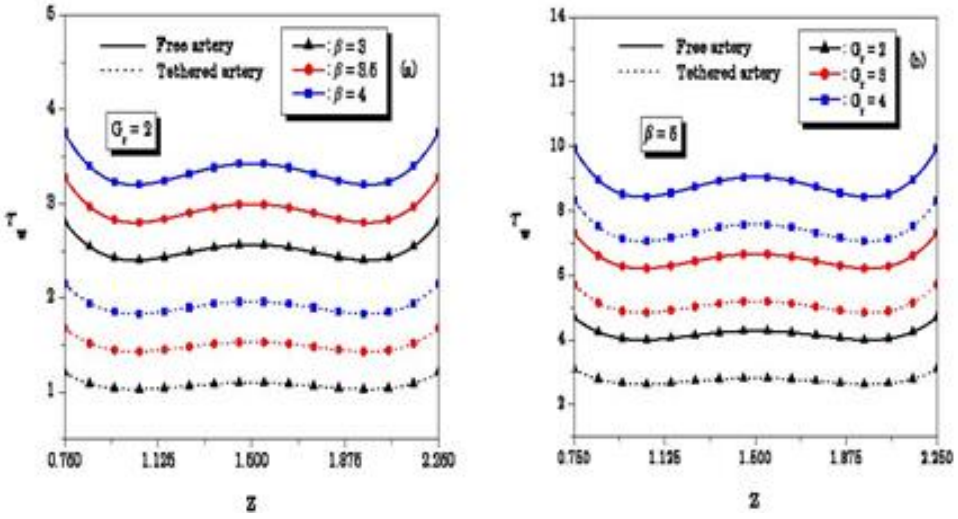

Figure-8. Variation of wall shear stress distribution τ_w with stenotic region for β and G_r at $t = 0.5,\ \delta^* = 0.1,$ $H_a = 2,\ \alpha = 45^o,\ S = 0.5,\ \varepsilon = 0.32,\ V_o = 0.1,\ e = 0.3,\ Z_o = 0.0001$ (panels (a) and (b) respectively).

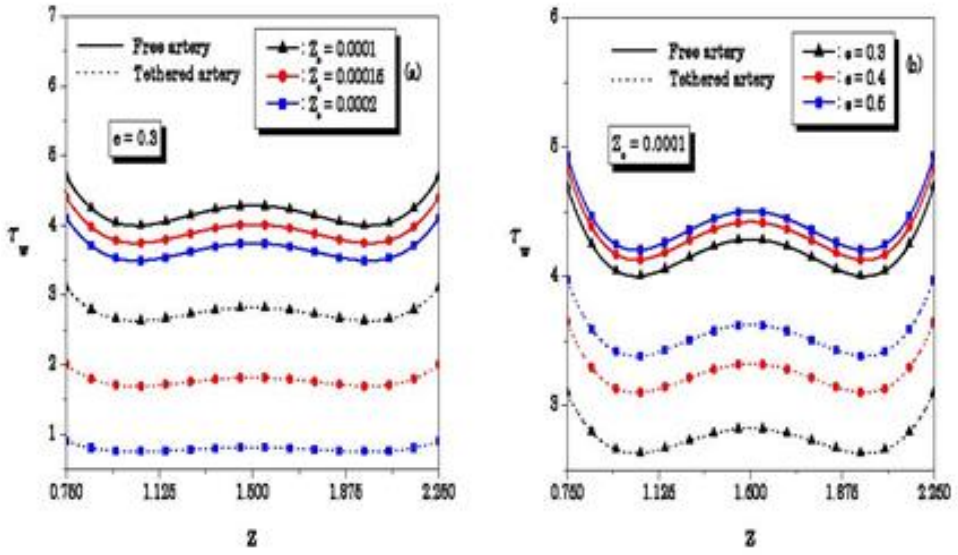

Figure-9. Variation of wall shear stress distribution τ_w with stenotic region for e and Z_o at $t=0.5,\ \delta^*=0.1,\ H_a=2,\ \alpha=45^o,\ S=0.5,\ \varepsilon=0.32,\ V_o=0.1,\ \beta=5,\ G_r=2$ (panels (a) and (b) respectively).

In Figure-10-a, the resistance impedance variance was displayed against Grashof number G_r for various values of heat source/sink parameter β. The results confirm a linear relation between the resistance impedance and free convection parameter. Moreover, the increase in the values of the free convection parameter leads to a decrease of the resistance impedance for the case of heat sink $(\beta=-5<0)$ or in the absence of heat source $(\beta=0)$ while it leads to an increase of the resistance in the case of heat source $(\beta=5>0)$. Figure-10-b explains the variance of resistance impedance λ with the magnetic parameter H_a for various values of inclination angle of magnetic field α. It is evident that the resistance increases with increases H_a when $\alpha=60^o, 90^o$ while at $\alpha=30^o$, the resistance impedance decreases with the small values of H_a but as the magnetic parameter H_a increases with greater values, the resistance will return increase.

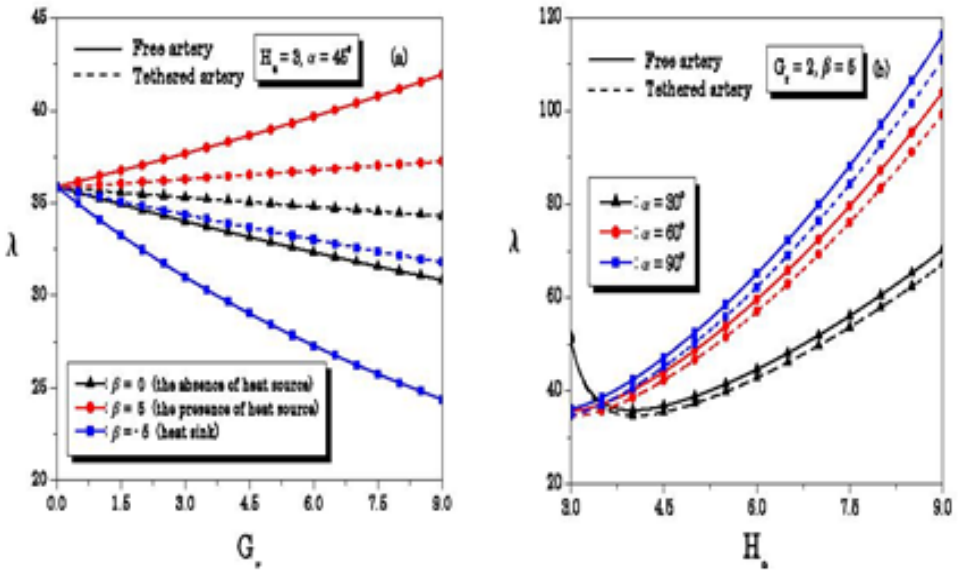

Figure-10. Variation of the resistance impedance λ with G_r and H_a for different values of β and α at $t=0.5,\ \delta^*=0.1,\ H_a=2,\ S=0.1,\ \varepsilon=0.32,\ V_o=0.1,\ e=0.3,\ Z_o=0.01$ (panels (a) and (b) respectively).

In Figures (11-12) variations of resistance impedance λ, with the maximum height of the stenosis δ^* have been studied for various values of catheter velocity V_o, radius of the catheter ε, the position of cilia Z_o, and the eccentricity of the elliptical path e. In Figure-11, the resistance impedance increases by increasing δ^*, V_o, and ε. Figure-12 explain the inverse change of resistance impedance with the position of cilia Z_o, and the eccentricity of elliptical path e where resistance impedance increases as the eccentricity of elliptical path e increases while it decrease by increasing the position of cilia Z_o. Figures (11-12) also illustrate that the resistance impedance curves are always higher in the case of the free artery model than in the tethered artery model.

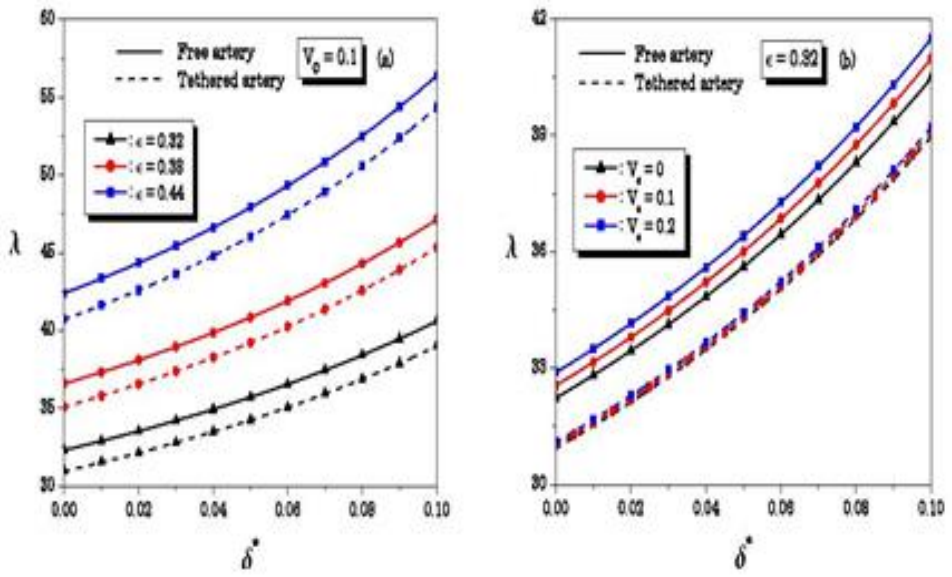

Figure-11. Variation of the resistance impedance λ with δ^* for different values of ε and V_o at $t=0.5,\ \alpha=45^o,\ H_a=5,\ S=0.5,\ \beta=5,\ G_r=2,\ e=0.3,\ Z_o=0.01$ (panels (a) and (b) respectively).

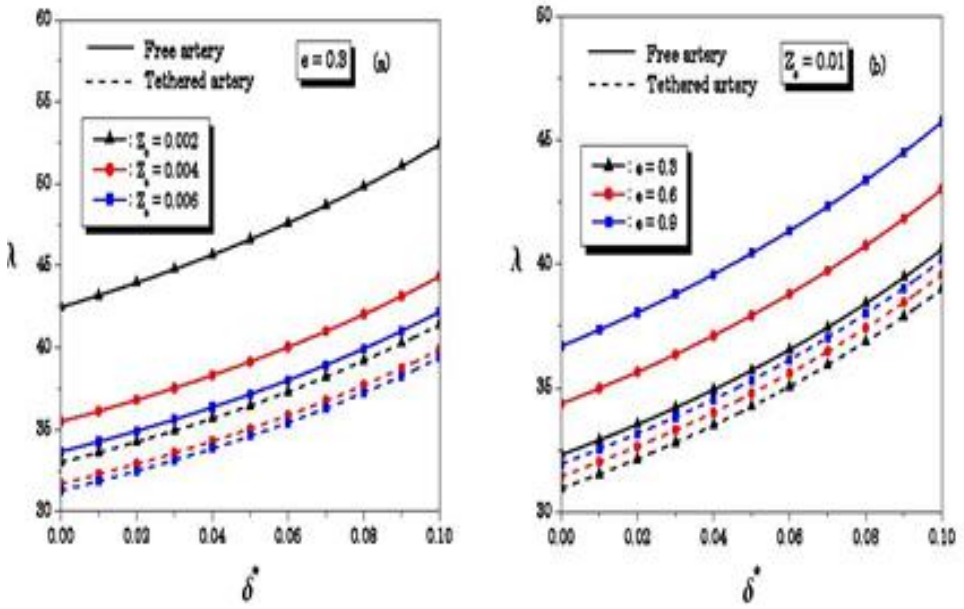

Figure-12. Variation of the resistance impedance λ with δ^* for different values of Z_o and e at $t=0.5,\ \alpha=45^o,\ H_a=5,\ S=0.5,\ \beta=5,\ G_r=2,\ \varepsilon=0.32,\ V_o=0.1$ (panels (a) and (b) respectively).

The variation of temperature profile with the heat source/sink parameter β, and the amplitude parameter of artery radius b was shown in Figure-13. It should be noted that the curves of temperature profile θ are always higher for steady wall case $(b=0)$ than in the case of the unsteady wall $(b=0.2)$ when the heat sink present or in the absence of the heat source $(\text{i.e. } \beta=-5<0 \text{ or } \beta=0)$ while the opposite occurs in the presence of the heat source $(\beta=5>0)$ (see Figure-13-a. Figure-13-b is prepared to see that the variation of temperature profile decreases rapidly for small values of the amplitude parameter of the artery $(0\le b\le 0.25)$ while it increases by increasing b in the interval $(0.25\le b\le 1)$. It is also noticed that the temperature curves θ increases by increasing the heat source/sink parameter β and the values of temperature are higher in the case of heat source $(\beta>0)$ than those in the case of heat sink $(\beta=0)$.

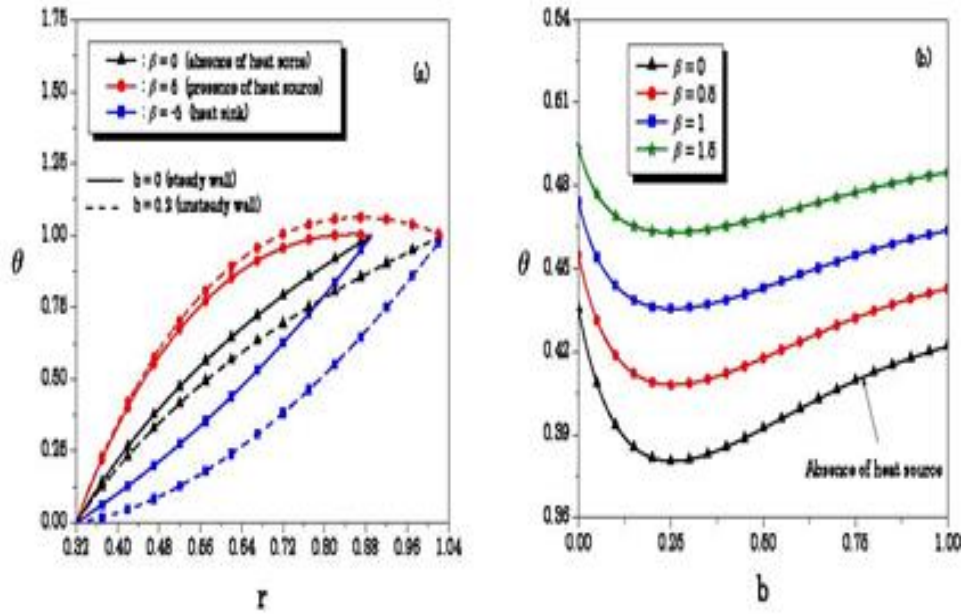

Figure-13. Variation of temperature distribution Θ with β and b (panel (a)) and with b for β (panel (b)) at $t=0.5,\ r=0.5,\ z=1.2,\ \delta^{*}=0.1,\ \varepsilon=0.32$.

Trapping phenomena has been shown in Figures (14-18) to depict the blood flow pattern in ciliated tethered stenosed artery. It is evident that more trapped bolus appears at the contraction area of the arterial wall. The size of trapping bolus increases as the position of cilia Z_o, the inclination angle of magnetic field α increase, and also when there exist heat sink or in the absence of heat source $(\text{i.e. } \beta<0 \text{ or } \beta=0)$whereas the size of trapping bolus decreases as the eccentricity of the elliptical path e and Grashof number G_r increase or in the presence of heat source $(\beta>0)$.

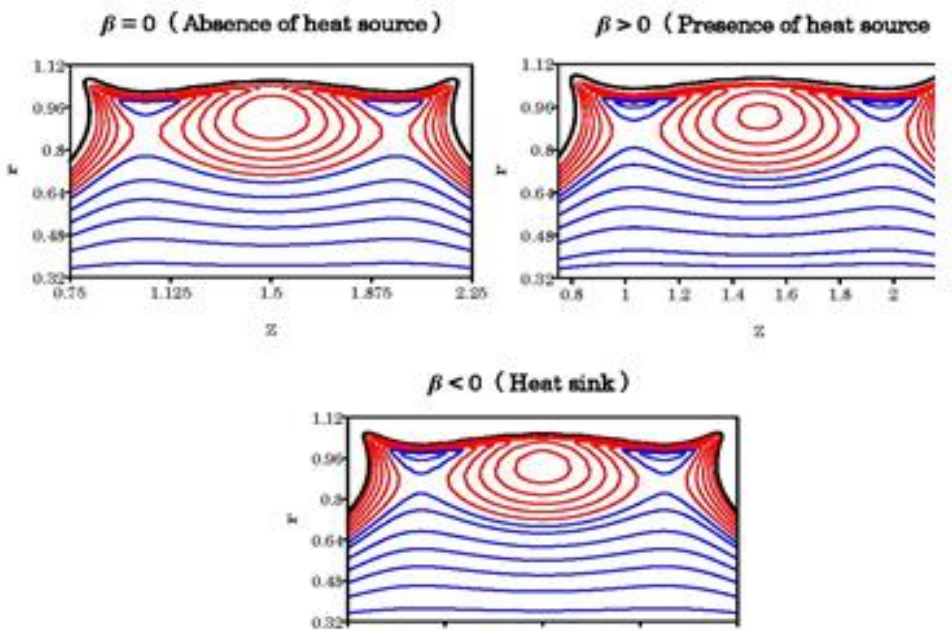

Figure-14. Plot showing streamlines for different values of the heat parameter at $t = 0.5,\ z = 1.2,\ \delta^* = 0.1,\ H_a = 2,\ \alpha = 45^o,\ S = 0.5,\ \varepsilon = 0.32,\ V_o = 0.1,\ e = 0.3,\ Z_o = 0.0001, G_r = 2.$

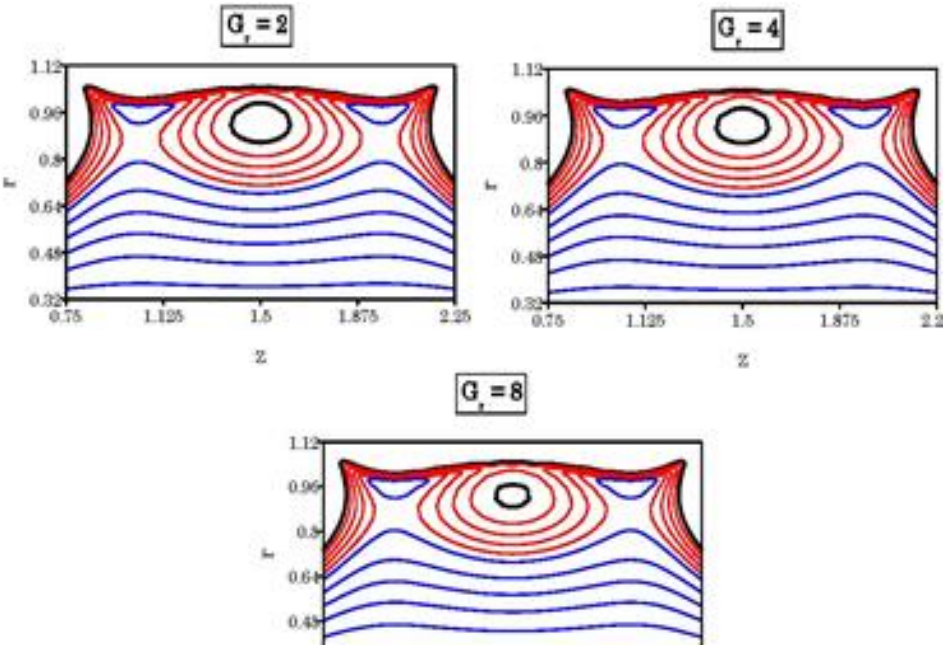

Figure-15. Plot showing streamlines for different values of Grashof number at $t = 0.5,\ z = 1.2,\ \delta^* = 0.1,\ H_a = 2,\ \alpha = 45^o,\ S = 0.5,\ \varepsilon = 0.32,\ V_o = 0.1,\ e = 0.3,\ Z_o = 0.0001,\ \beta = 5.$

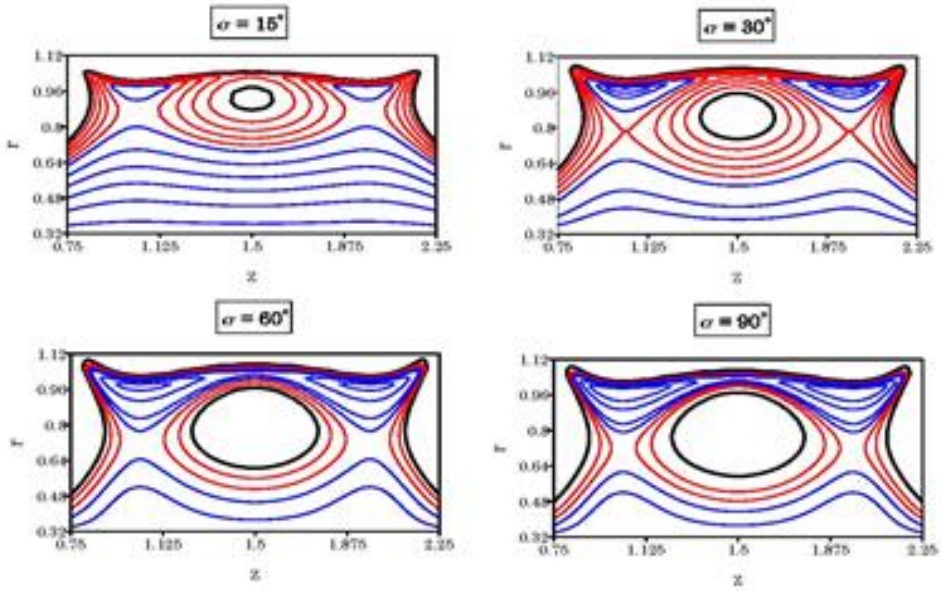

Figure-16. Plot showing streamlines for different values of inclination angle of magnetic field at $t = 0.5,\ z = 1.2,\ \delta^* = 0.1,\ H_a = 2,\ G_r = 2,\ S = 0.5,\ \varepsilon = 0.32,\ V_o = 0.1,\ e = 0.3,\ Z_o = 0.0001,\ \beta = 5.$

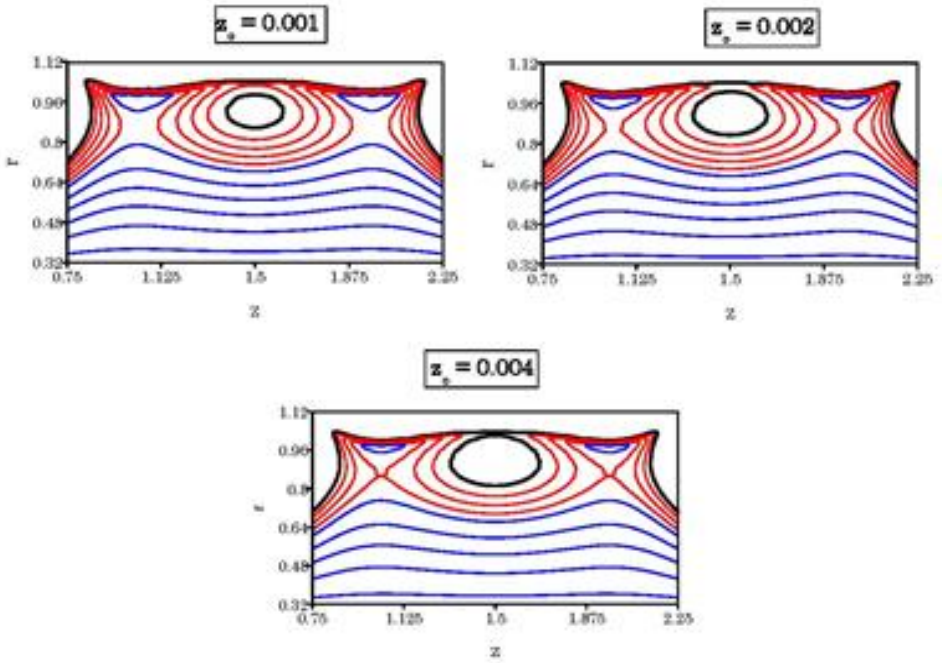

Figure-17. Plot showing streamlines for different values of the position of cilia at $t = 0.5,\ z = 1.2,\ \delta^* = 0.1,\ H_a = 2,\ \alpha = 45^o,\ G_r = 2,\ S = 0.5,\ \varepsilon = 0.32,\ V_o = 0.1,\ e = 0.3,\ \beta = 5.$

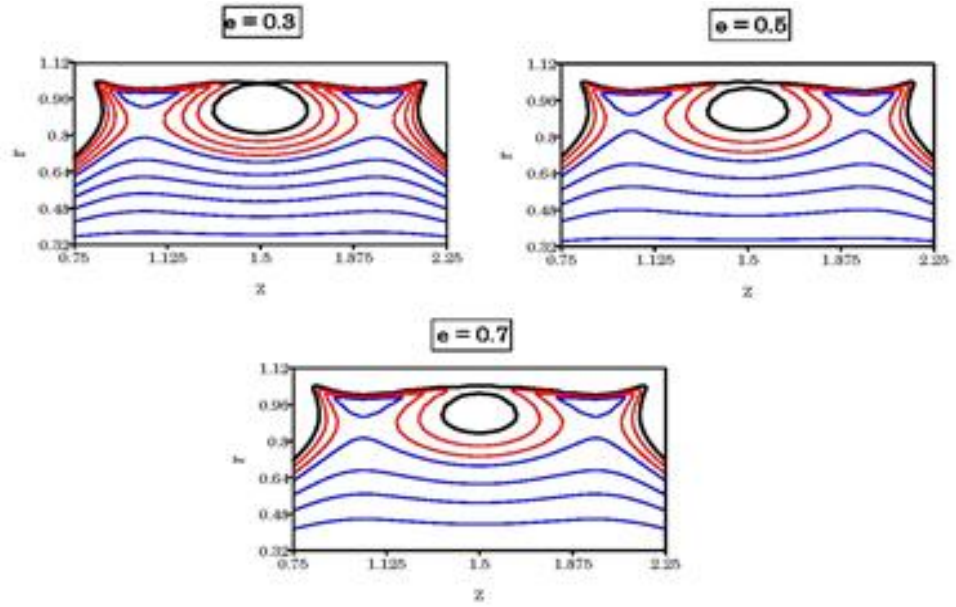

Figure-18. Plot showing streamlines for different values of the eccentricity of the elliptical path at $t = 0.5, z = 1.2, \delta^* = 0.1, H_a = 2, \alpha = 45^o, G_r = 2, S = 0.5, \varepsilon = 0.32, V_o = 0.1, \beta = 5, Z_o = 0.0001.$

4. CONCLUDING REMARKS

The effects of metachronal beating of cilia, heat transfer phenomenon, oblique magnetic field, and Hall currents on blood flow through catheterized anisotropically elastic arteries with overlapping stenosis are studied. This present study achieves some interesting results that can be summarized as follows: (1) The magnitudes of velocity, wall shear stress distributions, and resistance through free artery are always higher than these in tethered artery. (2) The transmission of velocity curves varies directly with the initial circumferential viscoelastic stress and increase significantly as the initial circumferential viscoelastic stress increase while it decreases as the anisotropy of the arterial wall, circumferential Poisson's ratio, and elastic constraints of total tethering increase. (3) The distribution of wall shear stress increases as cilia position increases and it decreases by increasing eccentricity of the elliptical path while the resistance impedance has inverse trend. (4) There is a linear relation between resistance impedance and free convection parameter. Moreover, the increasing of free convection parameter leads to decrease in resistance impedance in the case of heat sink or in the absence of heat source while it leads to an increase in the resistance of the resistance in the presence of heat source. (5) The resistance impedance decreases with the small values of magnetic parameter but as it increases with greater values, resistance will return to increase. (6) The temperature profile is always higher for steady arterial wall case than that in the case of unsteady arterial wall model when there exists heat sink or in the absence of heat source while the opposite happens in the presence of heat source. (7) The trapping bolus increases as the position of cilia, and the inclination angle of magnetic field increase also when there exists heat sink or in the absence of heat source while it decreases as the eccentricity of the elliptical path, and Grashof number increase or in the presence of heat source. (8) The trapping bolus increase clearly in the tethered artery while it does not appear clearly near the wall of free artery.

REFERENCES

[1] Chakravarty S., Ghosh Chowdhury A. 1988. Response of blood flow through an artery under stenotic conditions. Rheol. Acta. 27: 418-427.

[2] Velez-Cordero J. R., Lauga E. 2013. Waving transport and propulsion in a generalized Newtonian fluid. Journal of Non-Newtonian Fluid Mechanics. 199: 37-50.

[3] Ibaez-Tallon, I., Heintz, N., Omran H. 2003. To beat or not to beat: roles of cilia in development and disease. Hum. Mol. Genet. 1: 27-35.

[4] OCallaghan C., Sikand K., Chilvers M.A. 2012. Analysis of ependymal ciliary beat pattern and beat frequency using high speed imaging: comparison with the photomultiplier and photodiode methods. Cilia. 1: 1-8.

[5] Agrawal H. L., Anawaruddin. 1984. Cilia transport of bio-fluid with variable viscosity. Indian J. pure appl. Math. 15(10): 1128-1139.

[6] Akbar N. S., Khan Z. H. 2015. Metachronal beating of cilia under the influence of Casson fluid and

magnetic field. Journal of Magnetism and Magnetic Materials. 378: 320-326.

[7] Chiba R., Izumi M., Sugano Y. 2008. An analytical solution to non-axisymmetric heat transfer with viscous dissipation for non-Newtonian fluids in laminar forced flow. Arch. Appl. Mech. 78: 61-74.

[8] Hayat T., Umar Qureshi M., Hussain Q. 2009. Effect of heat transfer on the peristaltic flow of an electrically conducting fluid in a porous space. Applied Mathematical Modelling. 33: 1862-1873.

[9] Sarifuddin S., Chakravarty, Mandal, P.K. 2009. Effect of Heat and Mass Transfer to Blood Flow-Links to Atherosclerosis. International Journal of Heat and Mass Transfer. 52: 5719-5730.

[10] Sarifuddin, S., Chakravarty, Mandal, P. K, Andersson, H. I. 2009. Mass transfer to blood flowing through arterial stenosis. ZAMP. 60: 299-323.

[11] Ikbal A., Chakravarty S., Sarifuddin, Mandal P.K. 2010. Numerical simulation of mass transfer to micropolar fluid flow past a stenosed artery. International Journal for Numerical Methods in Fluids, DOI: 10.1002/fld.2438.

[12] Mekheimer Kh. S., Haroun Mohammed H., El Kot M. A. 2012. Influence of heat and chemical reactions on blood flow through an anisotropically tapered elastic arteries with overlapping stenosis. Appl. Math. Inf. Sci. 6(2): 281-292.

[13] Mekheimer Kh. S., El Kot M. A. 2012. Mathematical modeling of unsteady flow of a Sisko fluid through an anisotropically tapered elastic arteries with time-variant overlapping stenosis. Appl. Math. Modell. 36(11): 5393-5407.

[14] Mekheimer Kh. S., Elnaqeeb Thanaa, El Kot M. A., Alghamdi Felwah. 2016. Simultaneous effect of magnetic field and metallic nanoparticles on a micropolar fluid through an overlapping stenotic artery: blood flow model. Physics Essays. 29(2): 272-283.

[15] Ismail Z., Abdullah I., Mustapha N., Amin N. 2008. A power-law model of blood flow through a tapered overlapping stenosed artery. App. Math. and Comp. 195: 669-680.

[16] Chakravarty S., Datta A., Mandal P. K. 1995. Analysis of nonlinear blood flow in a stenosed flexible artery. Int. J. Engng. Sci. 33: 1821-1837.

[17] Chakravarty S. 1987. Pulsatile blood flow through arterioles. Rheol Acta. 26: 200-207.

[18] Atabek H. B., Lew H. S. 1966. Wave propagation through a viscous incompressible fluid contained in an initially stressed elastic tube. Biophysical Journal. 6: 481-503.

[19] Sleigh M. A. 1968. Patterns of ciliary beating: In aspects of cell motility. Soc. Expl. Biol. Symp. XXII. Academic press, p. 131. New York.

[20] Young D. F. 1968. Effect of a time dependent stenosis of flow through a tube. J. Eng. Ind. 90: 248-254.

[21] Kalita P., Schaefer R. 2008. Mechanical Models of Artery Walls, Arch Comput. Methods Eng. 15: 1-36.

[22] Womersley J. R. 1957. An elastic tube theory of pulse transmission and oscillatory flow in mammalian arteries. Wright Air Development Center Technical Report TR, 56-6114. Wright-Patterson AFB, Ohio.